Hydrogen-Bonding Interactions in the Binding of Loop 1 of Fasciculin 2 to *Torpedo californica* Acetylcholinesterase: A Density Functional Theory Study

Jing Wang,[†] Jiande Gu,*[,†,‡] and Jerzy Leszczynski*[,†]

Computational Center for Molecular Structure and Interactions, Department of Chemistry, Jackson State University, Jackson, Mississippi 39217, and Drug Design and Discovery Center, State Key Laboratory of Drug Research, Shanghai Institute of Materia Medica, Shanghai Institutes for Biological Sciences, Chinese Academy of Sciences, Shanghai 201203, People's Republic of China

Received: December 14, 2004; In Final Form: May 21, 2005

In the present study, the interactions of model complexes at the interface between loop1 of fasciculin 2 (Fas2) and acetylcholinesterase (AChE) are theoretically explored. Three interaction models based upon the crystal structure of the complex of Fas2 with AChE from *Torpedo californica* (PDB code 1FSS) were fully optimized at the B3LYP/6-311G(d,p) level of theory. The atoms-in-molecules (AIM) approach was employed to characterize the corresponding noncovalent hydrogen bonds through the densities and the Laplacians of electron densities at the bond critical points. The total interaction energy of loop 1 (Fas2) with AChE is predicted to be −99.4 kcal/mol. It is concluded that the Fas2 residue Thr8, which contributes more than half of the total binding energy, plays the most important role among the three binding sites. The energy decomposition results through the Kitaura−Morokuma scheme suggest that the electrostatic term is the major component of the entire interaction energy. The positive cooperativity effect revealed in the Thr8(F)-related models was confirmed through the geometry characteristics, AIM results, and the energy decomposition analysis.

Introduction

Enzymes are catalysts that change the rate of a reaction without being changed themselves. Enzymes are highly specific, and their activity can be regulated. Acetylcholinesterase (AChE)[1,2] (EC No. 3.1.1.7) belongs to the group of serine hydrolases. Through catalyzing the breakdown of the neurotransmitter acetylcholine (ACh), it terminates synaptic transmission at cholinergic synapses. The great speed of the enzyme is fundamental for rapid modulation of synaptic activity. The X-ray crystallographic structure of AChE[3] reveals a narrow and deep gorge that has two separate ligand binding sites:[4] the acylation site and the peripheral site (Figure 1). The acylation site lies at the bottom of the gorge, consisting of a catalytic triad (His440, Glu327, and Ser200), and the peripheral site is located at the entrance of the gorge. Ligands can bind selectively to either the acylation site or the peripheral site. During the catalytic process, an acyl-enzyme intermediate is formed at the acylation site. Certain cationic inhibitors, such as edrophonium and tacrine, bind selectively to this site.[5] Others, like propidium and fasciculin 2, bind to AChE at the peripheral site[6−8] and may interfere with the catalysis process of the enzyme through steric blockade of some ligands ingress to and egress from the acylation site.

Fasciculin2 (Fas2),[9,10] extracted from green mamba venom, is a selective peptidic inhibitor of AChE. It possesses 61 residues with four disulfide bridges. The overall net charge of Fas2 is +4 at a neutral pH. Structurally, Fas2 features three loops. Loop 1 is located between Cys3 and Cys17, containing 13 residues. Loop 2 lies between Cys22 and Cys39, containing 16 residues.

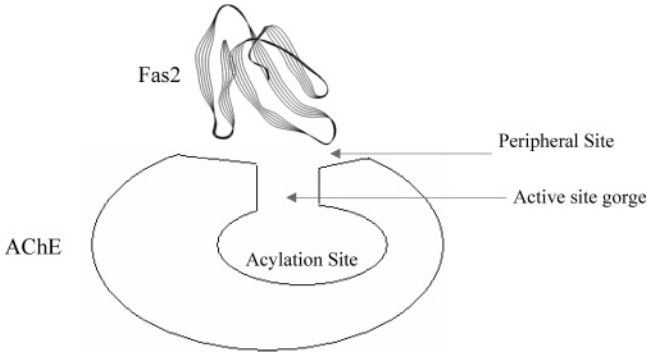

Figure 1. Schematic representation of Fas2 binding on the peripheral site of AChE.

Loop 3 of Fas2 is located between Cys41 and Cys52, encompassing 10 residues. With these loops, Fas2 binds tightly to mammalian and fish AChE at the peripheral site.[7,11]

A deeper understanding of the chemistry of the Fas2−AChE complex requires a functional map of the binding surfaces. Affinity labeling[12] and site-directed mutagenesis techniques[13,14] have been effectively employed to inspect the individual contributions of the fasciculin and acetylcholinesterase residues to complex formation and conformation. The availability of the crystal structures of the Fas2−AChE complexes offers insights into the detailed interaction patterns of the toxin and its target site. The recently solved X-ray structures of the Fas2-mouse−AChE (mAChE) (PDB code 1MAH),[15] Fas2-*Torpedo californica*−AChE (TcAChE) (PDB code 1FSS),[16] and Fas2-human−AChE (HuAChE) (PDB codes 1F8U and 1B41)[17] complexes display similar binding sites of loop 1 of Fas2. Due to the identical binding patterns of loop 1 of Fas2 with different AChEs, comparable binding properties might be expected for the above three different complexes. Three domains of Fas2

* Authors to whom correspondence should be addressed. E-mail: jiandegush@go.com; jerzy@ccmsi.us.
[†] Jackson State University.
[‡] Chinese Academy of Sciences.

10.1021/jp044302p CCC: $30.25
Published on Web 06/24/2005

anchor it to the enzyme, and a large contact area is revealed, consistent with the low dissociation constant of the complexes. This enables the Fas2 and AChE residues that participate in the interactions at the binding interfaces to be labeled.

Fas2 was shown to affect the orientation of selected side chains lying at the base of the active center gorge of AChE and therefore lead to the allosteric control of AChE catalysis.[18] It was reported that steps involving proton transfer during enzyme acylation were slowed due to the altered conformation of the active site in the ternary complex caused by the binding of Fas2 to AChE.[19] Rosenberry's study demonstrated that the binding of Fas2 to the AChE peripheral site considerably reduces the association and dissociation rate constants for *N*-methylacridinium binding to the active site.[20] The steric blockade model of the neurotoxin fasciculin and AChE was examined by Szegletes, suggesting that the peripheral site of AChE serves as an initial binding site for substrate entry to the acylation site and that this initial binding accelerates the rate for substrate hydrolysis at low substrate concentrations.[21] Comparative analysis of the kinetics of ligand entry and exit from the active center gorge for free AChE and the Fas2−AChE complex reveals that Fas2 influences the catalytic parameters by a more complex mechanism than simple restriction of diffusional entry and exit from the active center, and conformational flexibility appears critical for facilitating ligand passage in the narrow active center gorge.[22] It has been suggested that fasciculin alters the activity of mAChE by altering the dynamics and the structure of the enzyme, particularly of the large Ω loop. This loop undergoes a flexible rearrangement during which some of its secondary structure rapidly interchanges from a coil to a 3−10 or α-helix segment. Enhanced interactions well beyond the Trp286 P-site provide a structural basis for an inhibitory conformational effect on the A-site. Displacements of the large Ω loop appear to favor alternate routes of access to the enzyme's active site. [23] The nanosecond dynamics of the mAChE Cys69−Cys96 Ω loop were studied in the absence and presence of two inhibitors of different size, P-site inhibitor fasciculin and active site inhibitor huperzine. The residues in the Ω loop exhibit distinctive conformational fluctuations and therefore are likely to contribute to transient gorge enlargements in the free enzyme.[24] Molecular dynamics simulation approaches have been applied to explore the inhibition of mAChE by Fas2, assuming the combined mechanism of allosteric and dynamic inhibiting action.[25] Site-directed mutagenesis[13,26] implies that, among the residues of Fas2 that are close to AChE, only a small portion provides the critical contacts with AChE. Marchot et al.[26] have investigated 16 Fas2 mutants for T8A/T9A and R11Q on loop 1, R24T, K25L, R27W, R28D, H29D, Δpro,[30] P31R, K32G, M33A, and V34A/L35A on loop 2, and D45K and K51S on loop 3. Their results reveal that the Arg27, Pro30, and Pro31 mutants at the tip of loop 2 dominate the loop conformation and interaction of Fas2 with the enzyme and that the Arg24 and Met33 mutants make moderate contributions to the strength of the complex. In addition, the Thr8/Thr9, Arg11, and His29 mutants were considered to be immunochemical determinants in these regions or intramolecular rearrangements in conformations that enhance the interaction. The other 7 mutants left caused virtually no effect on Fas2 activity. From the analytical approach of interatomic contacts of structural units (CSUs) on the Fas2−TcAChE complex (PDB code 1FSS),[27] Fas2 residues from His6 to Ala12 in loop 1 were observed to contact with three segments of AChE, Gln68−Gly77, Glu82−Met90, and Gln272−Trp279. Among these contacting residues, Fas2 residues of His6, Thr7, Thr9, and Ser10 mainly display the typical hydrophobic−hydrophilic interactions that destabilize the combined Fas2−TcAchE complex. Fas2 residues Thr8, Arg11, and Ala12 reveal both hydrophilic−hydrophilic interactions (hydrogen bonding) and hydrophobic−hydrophobic interactions. These three residues occupy about 65% of the contact surface, whereas Thr8 and Arg11 contribute more than 53% of the total contact surface area at the loop 1 interface of Fas2, implying that the two residues might dominate the interaction between loop 1 and AChE.

Noncovalent interactions, including hydrogen bonding, dispersion interactions, electrostatic interactions, hydrophobic interactions, charge-transfer interactions, and ion-mediated interactions, play dominant roles in protein conformation and the folding process.[28,29] Among them, hydrogen bonding has been recognized as one of the most important interactions in biosystems.[30,31] The coexistence of several pairs of hydrogen bonds is common in protein−protein complexes. Due to the coupling between hydrogen bonds, their cooperativity becomes a feature of primary importance.[32] Cooperativity of hydrogen bonding has been found to directly tighten or loosen the bound protein complexes by increasing or decreasing the individual hydrogen-bonding interactions. [33−39] Accordingly, the possible cooperativity effects are expected to be of significant importance for the interactions of Fas2 and AChE. This topic should be addressed in both the experimental and the theoretical studies.

Experimental investigations have outlined the interactions of Fas2 and AChE. However, they do not reveal clearly to what extent each contact residue between Fas2 and AChE contributes to the overall binding energy. A detailed interaction energy characterization of the binding site is indispensable for a better understanding of the binding of Fas2 on the AChE peripheral site and, accordingly, the inhibition influences on the active catalytic function of AChE. Only nonempirical theoretical calculations could reveal details of such interactions. However, the considered species are too large for ab initio calculations. To study them at the desired level of theory, we consider a series of model complexes of increasing complexity that mimic the important parts of the real biological system. Though in such models some properties of the protein−enzyme interactions are neglected, they allow the study of individual contributions and the investigation of the development of the cooperative effects. We do expect that such a study provides reliable information on the binding trends despite the fact that the total energies are not accurate due to the simplifications of the models. In the present study, the hydrogen-bonding interactions at the interface between loop 1 of Fas2 and AChE are theoretically probed. Ab initio quantum chemical calculations were performed on the models, which are based upon the crystal structure data of the Fas2−TcAChE complex. The atoms-in-molecules (AIM) theory was employed to characterize the corresponding noncovalent hydrogen bonds. An energy decomposition analysis was applied subsequently to investigate the relative contributions of various energy terms (electrostatics, exchange repulsion, polarization, charge transfer, etc.) toward the total intermolecular interaction energy. The cooperative effects in model_III are elucidated through the geometric properties, AIM analysis, and energy decomposition approaches.

Methods

The local minima of the interactive models have been fully optimized by analytic gradient techniques. The method used was the density functional theory (DFT) with Becke's three parameter (B3)[40] exchange functional along with the Lee−Yang−Parr (LYP) nonlocal correlation functional (B3LYP).[41,42]

The standard valence triple-ζ basis set augmented with d-type and p-type polarization functions, 6-311G(d,p)[43] was used for all elements. It is well-known that the geometries and frequencies of the molecules calculated at the B3LYP/6-311G(d,p) level agree well with experiment.[44,45] Our previous studies of hydrogen-bonded biological systems have shown that the B3LYP approach predicts reliable structures and interaction energies and is compatible with the MP2/6-31(d,p) method.[46−48] In the calculations of harmonic vibrational frequency, the force constants were determined analytically for all of the complexes. In addition, the second order of the Møller−Plesset perturbation theory (MP2)[49−51] was applied to perform the single-point calculations at the B3LYP/6-311G(d,p)-optimized geometries. All ab initio calculations were carried out using the Gaussian 98 package of programs.[52]

The AIM theory of Bader[53,54] was applied to distinguish the hydrogen-bonding interactions in the interactive models. Eight topological criteria for the existence of hydrogen-bonding interactions were indicated by Koch and Popelier. Among them, the electronic density and the Laplacian of the density at the bond critical points (BCPs) are most often applied. They have been proven a useful tool in the study of hydrogen-bonding patterns. The electron density and the Laplacian at the BCPs for the H−Y contact within the X−H···Y−H bond should have a relatively high value. Both parameters for closed-shell interactions as hydrogen bonds are positive and should be within the following ranges: 0.002−0.04 au for the electron density and 0.02−0.15 au for the Laplacian.[55,56] In this study, the AIM analysis is based on the density obtained at the B3LYP/6-311G-(d,p) theoretical level. All the AIM analysis was carried out by AIM2000 program (version 2.0).[57]

Through the Kitaura−Morokuma scheme,[58,59] the interaction energies of the studied models were appropriately decomposed into their individual components to evaluate the contributions of the electrostatics, exchange repulsion, polarization, and other intermolecular interactions. The Morokuma decompositions were carried out by the GAMESS program[60] employing the 6-311G(d,p) basis set.

Results and Discussions

Model Construction. The models in this study were built upon the crystal structure of TcAChE complexed with Fas2 (PDB code 1FSS),[16] and the corresponding analysis resulted from the interatomic CSUs.[27] Model selections were constrained within the hydrophilic−hydrophilic contact (hydrogen bond) residues at the interface of loop 1 of Fas2, which stabilize the binding of Fas2 and TcAChE. The investigated interaction complexes were constructed to account only for isolated components.

Three residues (Thr8, Arg11, and Ala12) from loop 1 of Fas2 reveal close contacts with AChE residues via hydrogen-bonding interactions. Therefore, three corresponding interaction models were constructed as follows: model_I for the interactions of Fas2 residue Ala12 (Ala12(F)) with AChE residue Glu73 (Glu73(A)), model_II for Arg11(F) with an AChE fragment (including residues of Ser81(A), Glu82(A), Met83(A), Trp84-(A), and Asn85(A)), and model_III for Thr8(F) with AChE residues Tyr70(A), Val71(A), and Asp276(A) (Figure 2).

To reduce the computational demands, the considered models have been simplified. In model_II, the R-group of the Arg11-(F) residue was replaced by a methyl group. The side chains of the Met83(A) and Trp85(A) residues in model_II were truncated because these side chains are far away from the interface of loop 1 of Fas2 and only have insignificant influence on the interactions of these two moieties. In model_III, the neighboring amino acid that connects with O46 was replaced by a hydrogen atom.

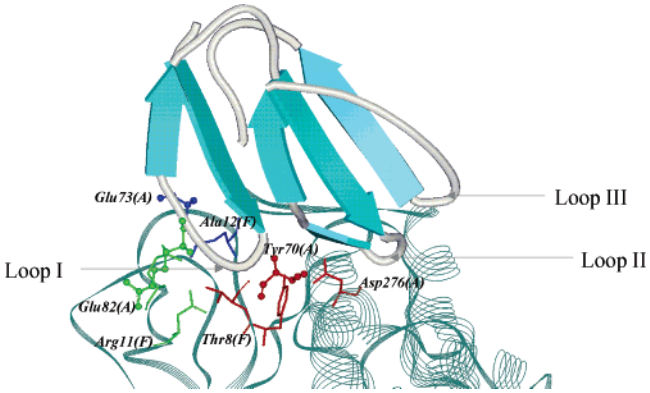

Figure 2. Interface contact pairs located at loop 1 of Fas2. Fas2 is shown in schematic display, and AChE in line ribbon. Residues from AChE are shown in ball and stick style, and residues from Fas2 in stick style. Model_I is shown in blue, model_II in green, and model_III in red.

TABLE 1: Bond Lengths, Bond Angles, Densities, and Laplacians of Densities at BCPs for Hydrogen Bonds in Interaction Models

	hydrogen bond	hydrogen-bond length (Å)	bond angle (deg)	ρ	$\nabla^2\rho$
model_I	C22H27···O9	2.349	129.6	0.0136	0.0427
	N18H23···O8	1.993	171.8	0.0249	0.0804
	C2H11···O8[a]	2.134	128.1	0.0213	0.0706
model_II	N50H60···O12	1.746	154.9	0.0412	0.1277
	C56H58···O12	2.568	135.1	0.0091	0.0274
	N51H54···O7	2.157	143.4	0.0154	0.0581
	N50H52···O7	2.135	143.4	0.0174	0.0629
	N51H53···O36	2.042	151.1	0.0207	0.0752
	N48H55···O36	2.146	145.7	0.0153	0.0593
	C56H58···O11	2.726	137.5	0.0065	0.0201
	N40H45···O11[a]	1.812	167.0	0.0334	0.1194
	C37H43···O11[a]	2.508	138.8	0.0086	0.0291
	C5H14···O11[a]	2.284	134.6	0.0155	0.0490
model_III	O48H53···O34	1.706	176.7	0.0449	0.1334
	N43H50···O35	1.704	162.7	0.0471	0.1317
	O12H20···O42	1.783	163.1	0.0341	0.1230
	N21H24···O46	2.031	170.4	0.0204	0.0745
	N29H36···O34[a]	1.983	128.8	0.0267	0.0957

[a] Intramolecular hydrogen bonds.

Geometric Properties. The three interactive models have been fully optimized at the B3LYP/6-311G(d,p) theoretical level. Frequency analysis at the same calculation level suggests that all structures are local energy minima on the potential energy surface. For hydrogen-bonded interactions revealed in the models, the corresponding geometric parameters (hydrogen-bond lengths and hydrogen-bond atomic angles), the electronic densities, and the Laplacian of the electron density at the hydrogen-bond BCPs (from the AIM analysis) are detailed in Table 1.

Model_I describes the interaction between Ala12(F) and Glu73(A). The Glu73(A) residue has a negative charge around its carboxylic group. The atomic distance of H27 from Ala12-(F) and O9 from Glu73(A) is predicted to be 2.349 Å, suggesting a CH···O hydrogen-bonding interaction, which is also indicated by a BCP density of 0.0136 au. A strong NH···O-type hydrogen bond has been predicted between O8 of Glu73(A) and H23 of Ala12(F), with a shorter bond distance of 1.993 Å and a larger BCP density of 0.0249 au.

A medium intramolecular hydrogen-bonded interaction was revealed for the AChE moiety in model_I, where H11 interacts

with O8 from the nearby carboxylic group with an atomic distance around 2.134 Å and a density of BCP at 0.0213 au, contributing to the stabilization and folding of the AChE fragment.

Model_II contains the residue Arg11(F) of Fas2 and the peptide chain of Ser81(A) through Asn85(A) from AChE, illustrating the simultaneous interaction of Arg11(F) with Glu82-(A) and Asn85(A).

The Glu82(A) extremity in model_II shows a tighter binding with Fas2 than the Glu85(A) end. The negatively charged carboxyl and the oxygen atom from the acyl group of Glu82-(A) provide the main contributions to the interactions with the Fas2 positively charged residue Arg11(F) in model_II.

Two pairs of bifurcated hydrogen bonds were formed at the Glu82(A) terminus. A NH···O bifurcated hydrogen bond was displayed for O7 of Glu82(A) with H54 and H52 of Arg11(F), which was indicated by the values of the atomic distances (2.157 Å vs 2.135 Å) and the densities of the BCPs (0.0154 au vs 0.0174 au). Another bifurcated hydrogen bond was revealed at the negatively charged R-group carboxylate. O12 of Glu82(A) interacts simultaneously with H58 and H60 of Arg11(F), leading to a medium CH···O-type and a strong NH···O hydrogen bond, with hydrogen-bond lengths of 2.568 and 1.746 Å and densities at the BCPs of 0.0091 and 0.0412 au, respectively.

Besides the contributions of O12 from the carboxyl group to the hydrogen bonds described above, another oxygen atom (O11) also participates in a slightly weaker CH···O hydrogen-bonded interaction with H58 of Arg11(F), as proven by the hydrogen-bond atomic distance of 2.726 Å and a BCP density of 0.0065 au.

Furthermore, O11 of Glu82(A) takes part in the formation of three intramolecular hydrogen bonds with H43, H14, and H45. These intramolecular hydrogen bonds are contributing to the folding of the AChE segment and cause contraction of this biomolecule.

At the other end of the peptide chain of AChE, the Asn85-(A) residue appears to bind more loosely with the Arg11(F) residue than Glu82(A). Only O36 of Asn85(A) was noticed to form a strong bifurcated NH···O hydrogen bond with H53 and H55 of Arg11(F), as verified by the atomic distances of 2.042 and 2.146 Å and the densities of the BCPs of 0.0207 and 0.0153 au, respectively.

Model_III demonstrates the collaborative interactions among the Fas2 residue Thr8(F) and the AChE residues of Tyr70(A), Val71(A), and Asp276(A).

Asp276(A) has a negatively charged R-group carboxylate. With an atomic distance of 1.704 Å and a density at BCP of 0.0471 au for O35 of the carboxylic group and H50 of Thr8-(F), a strong NH···O-type hydrogen bond is expected. Another oxygen atom (O34) of the carboxylic group was revealed to form a strong OH···O hydrogen bond with the hydroxyl H53 of Thr8(F) by a short atomic distance of 1.706 Å together with a large BCP density of 0.0449 au. Meanwhile, the prediction of a bond length of 1.983 Å and a BCP density of 0.0267 au between O34 and H36 inside the Asp276(A) segment implies a medium NH···O intramolecular hydrogen-bonding interaction that stabilizes this moiety.

As for the other part of the interacting fragments of model_III, which includes residues of Tyr70(A), Val71(A), and Thr8(F), a medium NH···O hydrogen bond was detected between O46 of Thr8(F) and H24 of Val71(A), with an atomic distance of 2.031 Å and a BCP density of 0.0204 au. A strong hydrogen bond was also detected for the acyl O42 of Thr8(F) and the H20 of Tyr70(A); the bond length and the BCP density are measured to be 1.783 Å and 0.0341 au, respectively.

TABLE 2: Interaction Energies and Gibbs Free Energies of the Three Interaction Models

	ΔE (kcal/mol) B3LYP	ΔE (kcal/mol) MP2[a]	$\Delta E°$ (kcal/mol) B3LYP	$\Delta G°_{298}$ (kcal/mol) B3LYP
model_I	−18.9	−22.1	−17.4	−6.8
model_II	−30.0	−33.2	−27.6	−13.1
model_III	−58.3	−65.1	−55.0	−31.8
total	−107.2	−120.4	−100.0	−51.7

[a] Single-point energy calculations at the MP2/6-311G(d,p) level for the B3LYP/6-311G(d,p)-optimized geometries.

Energy Properties. The B3LYP/6-311G(d,p) level interaction energies and zero-point corrected interaction energies for the three studied models are summarized in Table 2. The calculated Gibbs free energies of the formation of the models at 298 K, including vibrational contributions in the harmonic approximation, together with the single-point energy calculations at the MP2/6-311G(d,p) level for the B3LYP/6-311G(d,p)-optimized geometries, are also listed in Table 2.

Among the three models, the interaction energy for model_I is calculated to be −18.9 kcal/mol (−17.4 kcal/mol after a zero-point correction) at the B3LYP/6-311G(d,p) theoretical level. The single-point energy calculation resulting from a higher level for model_I (MP2/6-311G(d,p)) increased this value to −22.1 kcal/mol. The Gibbs free energy at 298 K for the binding of model_I is predicted to be −6.8 kcal/mol.

With three pairs of bifurcated intermolecular hydrogen bonds, model_II is characterized by a larger binding energy of −30.0 kcal/mol (−27.6 kcal/mol after the zero-point correction and −33.2 kcal/mol at the MP2 level). The Gibbs free energy of the formation of model_II at 298 K is more negative (−13.1 kcal/mol), indicating a tighter binding of model_II than model_I.

For model_III, the Thr8(F) residue collaboratively binds with two pieces of the ligand, Asp276(A) and Tyr70(A)/Val71(A). The interaction energy for model_III amounts to −58.3 kcal/mol (−55.4 kcal/mol after the zero-point correction and −65.1 kcal/mol of MP2 level single-point calculation), revealing the strongest binding property among the three models. This is also indicated by the largest Gibbs free energy of formation of model_III at 298 K (−31.8 kcal/mol). Among all three models studied, model_III contributes more than half of the total binding energy of loop 1(Fas2) with AChE.

It should be noted that the interaction between the Thr8(F) residue and the Tyr70(A) residue (through O42 of Thr8(F) and H20 of Tyr70(A)) in model III (due to the existence of the hydroxyl group on the phenyl) has not been detected in original crystallographic data. To evaluate the effect of this interaction on the Thr8(F) binding site, one more model (model_IV in Figure 3) has been studied. In this model, we replaced the hydroxyl group of the phenyl with hydrogen to eliminate the above-mentioned extra hydrogen-bonding interaction displayed in model_III. The comparison of the optimized geometries of model_IV and model_III reveals that these two species display similar binding patterns for the Val71(A) and Asp276(A) residues with Thr8(F), which are characterized by three pairs of intermolecular hydrogen bonds (HB1, HB2, and HB3; Figure 3) and one intramolecular hydrogen bond (HB4; Figure 3). HB1, HB2, and HB4 have been predicted to be slightly stronger in model_IV than those in model_III, indicated by the shorter bond lengths (approximately 0.01−0.03 Å shorter) and the larger values of the BCP densities (approximately 0.001 au increase).

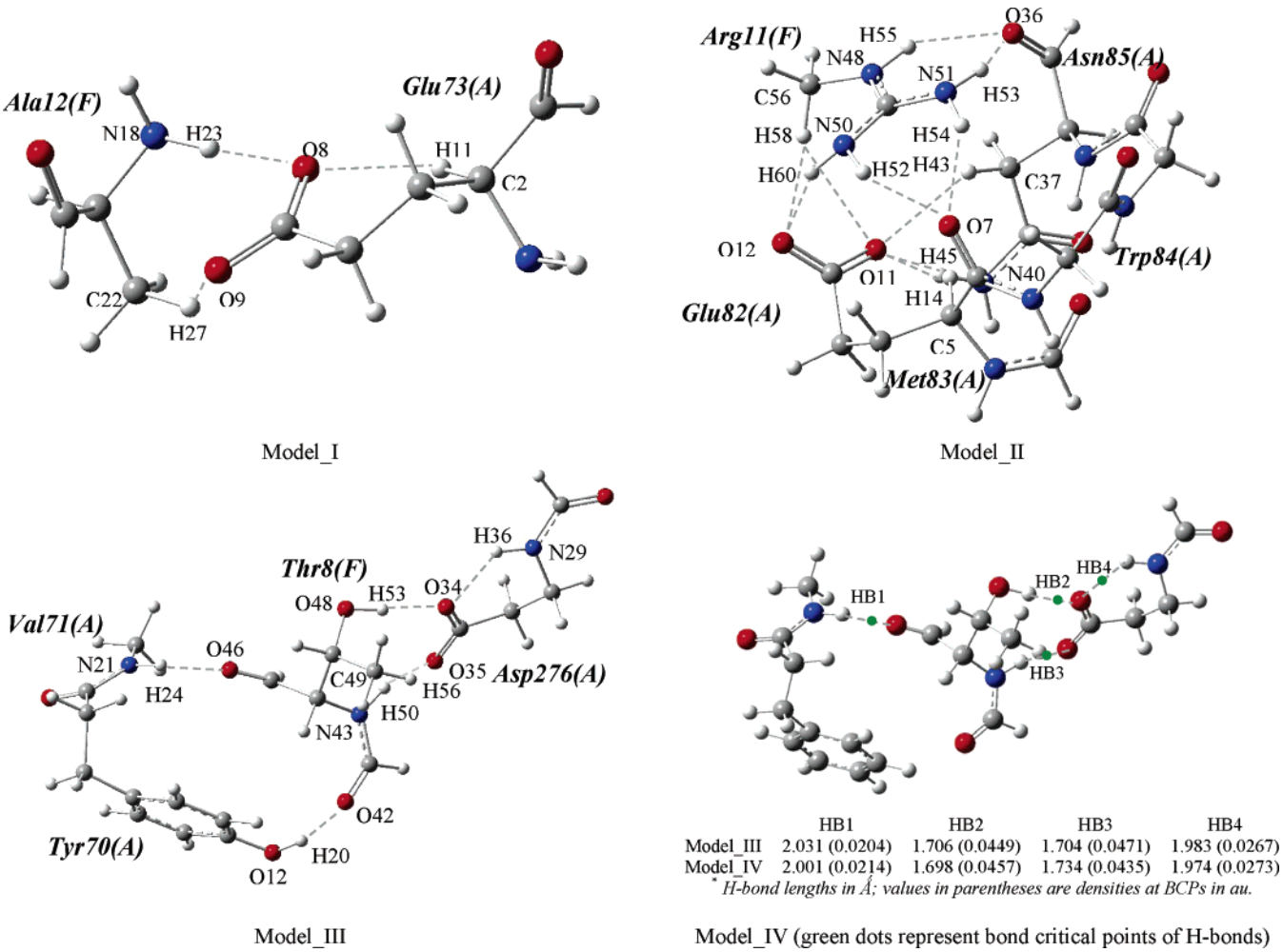

	HB1	HB2	HB3	HB4
Model_III	2.031 (0.0204)	1.706 (0.0449)	1.704 (0.0471)	1.983 (0.0267)
Model_IV	2.001 (0.0214)	1.698 (0.0457)	1.734 (0.0435)	1.974 (0.0273)

* *H-bond lengths in Å; values in parentheses are densities at BCPs in au.*

Figure 3. Optimized interactive models at the B3LYP/6-311G(d,p) level. Dashed lines represent hydrogen bonds. F and A in parentheses represent residues of Fas2 and AChE, respectively.

HB3 seems to be a little weaker in model IV; its bond length is about 0.03 Å longer, and the corresponding BCP value is about 0.001 au less as compared to those in model III. However, the binding energy of model_IV is evaluated to be −50.5 kcal/mol. In comparison with the binding energy of model_III (−58.3 kcal/mol), this suggests that the extra hydrogen-bonding interaction between Thr8(F) and Tyr70(A) contributes less than 8 kcal/mol to the total interactions of model_III. However, even after eliminating the influence of this extra hydrogen bond in model_IV, the Thr8(F) residue still plays the most important role among the three binding sites of loop 1 of Fas2.

According to the values of the interaction energies of the four models (model_I, model_II, model_III, and model_IV), the entire binding energy for loop 1 of Fas2 with AChE is evaluated to be −99.4 kcal/mol. Among the three binding sites at the interface of loop 1 in Fas2 (Ala12(F), Arg11(F), and Thr8(F)), the Thr8(F) and Arg11(F) residues dominate the loop 1(Fas2)−AChE interaction. The conclusion that the Thr8(F) residue plays the most important role among the three binding sites of loop 1 of Fas2 is consistent with the results from the interatomic CSU analysis.[27]

To obtain a clearer view of the interactions between Fas2 loop 1 and AChE, the classical Kitaura−Morokuma energy decomposition analysis was carried out to break down the interaction into electrostatic, exchange repulsion, and mixture components. Among the energy components, the electrostatic energy (ES) term represents the classical Coulombic force between the charge distributions of the two partner molecules;

TABLE 3: Interaction Energy Decomposition Results via the Kitaura−Morokuma Scheme[a]

	ES (kcal/mol)	EX (kcal/mol)	PL (kcal/mol)	mixture (kcal/mol)
model_I	−20.6	15.0	−6.7	−7.1
model_II	−125.2	32.7	−15.1	−10.9
model_III	−75.9	52.1	−18.8	−19.9

[a] ES, electrostatic term; EX, exchange term; PL, polarization term.

the exchange energy (EX) corresponds to the steric repulsion between the electron clouds of the two molecules, and the remaining components arise when the two molecules are permitted to perturb the electron clouds of one another, containing the contributions of polarization (PL) and charge transfer (CT). The Morokuma interaction energy decompositions of the three models presented here were derived based on the optimized structures at the B3LYP/6-311G(d,p) level.

The energy components of the interaction energies of the three models are reported in Table 3. Inspection of Table 3 suggests that the electrostatic energy is the largest attractive component in all three models. The only repulsive component is the exchange energy , which in all cases is smaller in magnitude than the ES. The polarization term and the mixture term containing the charge-transfer component provide smaller, but not insignificant, contributions to the total interaction energies, compensating mostly for the repulsive component of EX. Hence, it is obvious that the interactions between Fas2 loop 1 and AChE are mainly electrostatic.

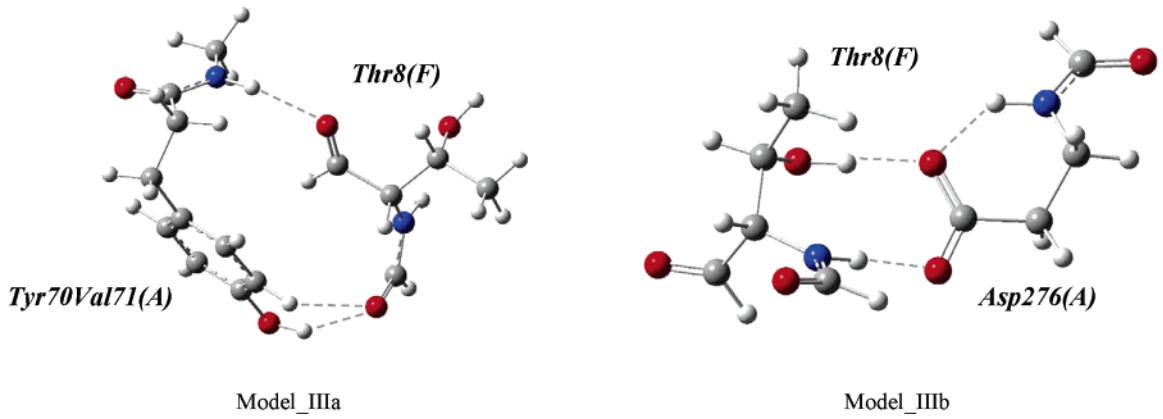

Figure 4. Optimized structures for model_IIIa and model_IIIb at the B3LYP/6-311G(d,p) level. The series number of atoms is the same as in model_III of Figure 3.

TABLE 4: Positive Cooperativity Revealed through Hydrogen-Bond Properties for Model_III

hydrogen bond	hydrogen-bond length (Å)	bond angle (deg)	ρ	$\nabla^2\rho$
O12H20···O42[a]	1.783 (1.938)	163.1 (148.6)	0.0341 (0.0243)	0.1230 (0.0919)
C9H18···O42[a]	2.579 (2.770)	117.9 (112.2)	0.0086 (0.0062)	0.0304 (0.0230)
N21H24···O46[a]	2.031 (2.110)	170.4 (161.9)	0.0204 (0.0176)	0.0745 (0.0618)
C49H56···O34[b,c]	2.784 (*3.049*)	118.2 (*101.1*)	0.0063	0.0230
O48H53···O34[b]	1.706 (*1.728*)	176.7 (*174.7*)	0.0449 (*0.0424*)	0.1334 (*0.1297*)
N43H50···O35[b]	1.704 (*1.760*)	162.7 (*165.1*)	0.0471 (*0.0403*)	0.1317 (*0.1220*)
N29H36···O34[d]	1.983 (*1.950*)	128.8 (*130.2*)	0.0267 (*0.0285*)	0.0957 (*0.1009*)

[a] Underlined values are from model_IIIa. [b] Italic values are from model_IIIb. [c] No such hydrogen bond was observed in model_IIIb. [d] Intramolecular hydrogen bond.

TABLE 5: Positive Cooperativity Effect Revealed through the Interaction Energy of Model_III

models	ΔE (kcal/mol)		$\Delta E°$ (kcal/mol)[a]	$\Delta G°$ (kcal/mol)[a]
	B3LYP	MP2[b]	B3LYP	B3LYP
model_IIIa[c]	−11.8	−17.2	−10.1	2.3
model_IIIb[d]	−38.2	−40.3	−36.3	−25.1
model_IIIa + model_IIIb[c,d]	−50.0	−57.5	−46.4	−22.8
model_III[e]	−58.3	−65.1	−55.0	−31.8

[a] $E°$, zero-point-corrected energy at the B3LYP/6-311G(d,p) level; G°, Gibbs free energy (298 K) at the B3LYP/6-311G(d,p) level. [b] Single-point energy calculations at the MP2/6-311G(d,p) level for the B3LYP/6-311G(d,p)-optimized geometries. [c] $\Delta E/\Delta E°/\Delta G°$ (model_IIIa) = $E/E°/G°$ (model_IIIa) − $E/E°/G°$ (Tyr70(A)/Val71(A)) − $E/E°/G°$ (Thr8(F)). [d] $\Delta E/\Delta E°/\Delta G°$ (model_IIIb) = $E/E°/G°$ (model_IIIb) − $E/E°/G°$ (Asp276(A)) − $E/E°/G°$ (Thr8(F)). [e] $\Delta E/\Delta E°/\Delta G°$ (model_III) = $E/E°/G°$ (model_III) − $E/E°/G°$ (Tyr70(A)/Val71(A)) − $E/E°/G°$ (Thr8(F)) − $E/E°/G°$ (Asp276(A)).

Cooperative Interaction Effects in Model_III. As discussed above, model_III presents a binding complex with the strongest interaction for Fas2 loop 1 with AChE. In model_III, the two fragments of the AChE moiety (Asp276(A) and Tyr70(A)/Val71(A)) are located on different sides of the Fas residue Thr8(F). The crystallographical data of Fas2-bound AChE illustrate that there is almost no interaction between these two fragments. The possibility of the contribution of cooperative effects should therefore be considered for model_III.

To provide more detailed insight into this phenomenon, two individual models were separated from model_III, namely model_IIIa and model_IIIb. Model_IIIa considers the interaction of Thr8(F) with Tyr70(A)Val71(A), while model_IIIb considers the interaction of Thr8(F) with Asp276(A) (Figure 4). To inspect the cooperative effects, the individual models and the whole model will be compared and analyzed by gradual variations of the geometries of the structures and the interaction energies.

Both model_IIIa and model_IIIb are optimized at the same theoretical level (B3LYP/6-311G(d,p)) as model_III. No imaginary frequency revealed in the harmonic vibrational frequency calculations for both models suggests that they are energy-minimized structures. AIM analysis was applied to both models to locate the densities and the Laplacian of the density at the hydrogen-bond BCPs. The geometry parameters for model_III, model_IIIa, and model_IIIb are summarized in Table 4. The interaction energies at the B3LYP/6-311G(d,p) level, the single-point energy calculation at the MP2/6-311G(d,p) level, and the Gibbs free energy of formation of the models at 298 K are reported in Table 5.

For model_IIIa, there are three pairs of hydrogen-bonding interactions, similar to the interactions of the corresponding fragment in model_III. However, the hydrogen-bond lengths become 0.02−0.20 Å longer, and the hydrogen-bond BCP densities are 0.0024−0.0098 au smaller than those in model_III. This indicates that the corresponding hydrogen bonds in model_IIIa are weakened, due to the weaker interactions of individual fragments with AChE. The interaction energy for model_IIIa amounts to only −11.8 kcal/mol (−10.1 kcal/mol after the zero-point correction and −17.2 kcal/mol at the MP2

TABLE 6: Morokuma Energy Decomposition Results for Model_III, Model_IIIa, and Model_IIIb[a]

	ES (kcal/mol)	EX (kcal/mol)	PL (kcal/mol)	mixture (kcal/mol)
model_III	−75.9	52.1	−18.8	−19.9
model_IIIa	−16.5	12.5	−2.1	−5.0
model_IIIb	−49.7	29.7	−10.6	−11.8
model_IIIa + model_IIIb	−66.2	42.2	−12.8	−16.7
model_III − model_IIIa − model_IIIb	−9.8	9.9	−6.1	−3.2

[a] ES, electrostatic term; EX, exchange term; PL, polarization term.

level). The Gibbs free energy at 298 K for the formation of this fragment is estimated to be positive (2.33 kcal/mol), implying weak binding of model_IIIa.

With respect to model_IIIb, the longer atomic distance (2.784 Å) and the lack of predicted BCP between the O34 atom of Asp276(A) and the H56 atom of Thr8(F) indicate that there are no hydrogen-bonding interactions at this site, which is obviously different from the results obtained for the corresponding part of model_III. In comparison to model_III, two pairs of weaker intermolecular hydrogen-bonding interactions are displayed for O48H53···O34 and N43H50···O35, with the atomic distances being 0.022 and 0.056 Å longer and with the BCP densities being 0.0025 and 0.0068 au smaller, respectively. Meanwhile, an intramolecular hydrogen bond was predicted for N29H36···O34 with a shorter atomic distance of 1.950 Å (1.983 Å in model_III) and a larger BCP density of 0.0285 au (0.0267 au in model_III). It can be concluded that the intermolecular hydrogen-bonding interactions are weakened, while the intramolecular hydrogen-bonding interactions are strengthened for the separated individual models. The binding energy for model_IIIb is calculated to be −38.2 kcal/mol (−36.3 kcal/mol after zero-point correction and −40.3 kcal/mol at the MP2 level). The Gibbs free energy of Model_IIIb at 298 K amounts to −25.1 kcal/mol, indicating a tighter binding of this model than model_IIIa.

All intermolecular hydrogen-bond lengths in model_IIIa and model_IIIb have been predicted to be longer than the corresponding hydrogen bonds in model_III. The AIM analysis displays smaller densities of BCPs and smaller Laplacians of densities for the hydrogen bonds in the individual models than those in the full model of model_III. This suggests that with the collaborative interactions of Tyr70(A)/Val71(A) and Asp276(A) with Thr8(F) the intermolecular hydrogen bonds are strengthened, and the whole considered structure is tightened.

However, the energy value of the collaborative interactive model_III is larger than the total interaction energy of the two separate interactions in model_IIIa and model_IIIb. When Thr8(F) interacts with Tyr70(A)/Val71(A) and Asp276(A) separately, the binding energies amount to −11.8 kcal/mol and −38.2 kcal/mol, respectively, where the total interaction energy is evaluated to be −50.0 kcal/mol (−46.4 kcal/mol after the zero-point correction and −57.5 kcal/mol at the MP2 level single-point calculation). However, for the collaborative full interaction in model_III, the interaction energy reaches −58.3 kcal/mol (−55.0 kcal/mol after the zero-point correction and −65.1 kcal/mol at the MP2 level), about 8.3 kcal/mol higher than the total interaction energy of the separate interaction subsets (7.6 kcal/mol at the MP2 level), suggesting an energy enhancement by the collaborative interactions. Moreover, the Gibbs free energy of the binding of model_III at 298 K also reveals a tighter binding of the full model that is expressed by an increase of 10 kcal/mol in energy.

Regarding the cooperativity effects clarified by Williams et al.,[31−33] when ligand binding is not cooperative, a protein receptor structure remains unchanged upon ligand binding.

TABLE 7: Contributions of Solvation Energy to the Binding Energy at the B3LYP/6-311G(d,p) Level

models	ΔE (kcal/mol)[a]	ΔE_{solv} (kcal/mol)[b]
model_I	−18.9	3.5
model_II	−30.0	−9.7
model_III	−58.3	−16.9
model_IIIa	−11.8	−3.5
model_IIIb	−38.2	−13.7
model_IIIa + model_IIIb	−50.0	−17.2

[a] In the gas phase. [b] PCM model, with $\epsilon = 78.39$ (water).

Positive cooperativity is accompanied by structural tightening in the complex, and the observed binding energy is greater when the interactions occur together than when they occur separately from each other. The negative cooperativity effect leads to the loosened structure, and the resultant binding energy is lower when the interactions occur together than when they occur in isolation. Therefore, a positive cooperative effect is predicted for model_III. Model_IV reveals the same positive coorperativity as model_III (about 5.4 kcal/mol enhancement in binding energy).

The application of an energy decomposition scheme enables us to further explore to what extent each energy component contributes to the total binding energy due to the positive cooperativity. The energy decomposition analysis results for model_III, model_IIIa, and model_IIIb through the Kitaura−Morokuma scheme are shown in Table 6. The total electrostatic energy, exchange repulsion, polarization, and the mixture terms of model_IIIa and model_IIIb are predicted to be −66.2, 42.2, −12.8, and −16.7 kcal/mol, respectively. In comparison with the energy components of model_III, it is expected that the contributions of the energy components to the increase of the interaction energy caused by the positive cooperative effects amount to −9.8, 9.9, −6.1, and −3.2 kcal/mol, for the electrostatic, exchange repulsion, polarization, and mixture terms, respectively. It can be seen that an increase in the total interaction energy due to the positive cooperativity is gained mainly from the contribution of the electrostatic component.

It is well-known that solvent effects are important in biosystems. To examine the potential role of solvent, the polarizable continuum model (PCM) self-consistent reaction field of Tomasi and co-workers with a dielectric constant $\epsilon = 78.39$ (water)[61] was applied for the gas-phase-optimized structures. The solvent-effect-corrected interaction energies are listed in Table 7. The obtained results display that the polar solvent reduces the interaction energies of the models considered. However, the relative order of the interaction energies remains unchanged, and the Thr8(F)-related model_III still dominates. It has been noticed that the solvent plays an important role in the binding of loop 1 of Fas2 and AChE. Nevertheless, this does not change the conclusions drawn from the above gas-phase calculation results.

It should be noted that the microsolvation effects could be very important in the protein−enzyme interactions. The inclusion of water molecules in the interactions between the residues might alter the residue−residue interaction patterns. However,

the investigation of the microsolvation effects deserves separate exploration and is beyond the scope of this study. Here, the solvation effects are limited only to the consideration of the polarizable continuum model for the gas-phase geometries.

Summary

In this study, three models, which were built upon the crystallographic data of TcAChE complexed with Fas2, were chosen to investigate the interactions at the interface of Fas2 loop 1 and AChE. The geometric properties of the structures optimized at the B3LYP/6-311G(d,p) level of theory are characterized by the hydrogen-bond lengths, the hydrogen-bond atomic angles, the BCP densities, and the Laplacians of the electron densities obtained via the AIM approach.

The total interaction energy of Fas2 loop 1 with AChE is predicted by the present study to be −99.4 kcal/mol at the B3LYP/6-311G(d,p) level. It is concluded that among the three interaction sites of the Fas2 residues Thr8(F) plays the most important role. It contributes more than half of the total interaction energy of loop 1 (Fas2) with AChE. The energy decomposition results through the Kitaura−Morokuma scheme suggest that the electrostatic interaction is the main contribution to the total interaction energy.

In comparison with the separate individual interaction models, model_III and model_IV are characterized by a tightened structure and enhancement of the interaction energy. A positive cooperative effect is therefore expected for model_III (model_IV), and it leads to a more than 8 kcal/mol (5 kcal/mol) increase in binding energies.

Acknowledgment. This work was supported by the Office of Naval Research (Grant No. N00034-03-1-0116), High Performance Computing Visualization Initiative (Grant No. W912HZ-04-C-0033), and the Army High Performance Computing Research Center under the auspices of the Department of the Army, Army Research Laboratory (Cooperative Agreement No. DAAD19-01-2-0014, the content of which does not necessarily reflect the position or the policy of the government, and no official endorsement should be inferred).

References and Notes

(1) Rosenberry, T. L. In *Advances in Enzymology*; Meister, A., Ed.; John Wiley & Sons: New York, 1975; Vol. 43, pp 103−218.
(2) Quinn, D. M. *Chem. Rev.* **1987**, *87*, 955−975.
(3) Sussman, J. L.; Harel, M.; Frolow, F.; Oefner, C.; Goldman, A.; Toker, L.; Silman, I. *Science* **1991**, *253*, 872.
(4) Taylor, P.; Lappi, S. *Biochemistry* **1975**, *14*, 1989−1997.
(5) Harel, M.; Schalk, I.; Ehret-Sabatier, L.; Bouet, F.; Goeldner, M.; Hirth, C.; Axelsen, P. H.; Silman, I.; Sussman, J. L. *Proc. Natl. Acad. Sci. U.S.A.* **1993**, *90*, 9031−9035.
(6) Karlsson, E.; Mbugua, P. M.; Rodrigues-Ithurralde, D. *J. Physiol.* **1984**, *79*, 232−240.
(7) Marchot, P.; Khelif, A.; Ji, Y.-H.; Masnuelle, P.; Bourgis, P. E. *J. Biol. Chem.* **1993**, *268*, 12458−12467.
(8) Barak, D.; Kronman, C.; Ordentlich, A.; Ariel, N.; Bromberg, A.; Marcus, D.; Lazar, A.; Velan, B.; Shafferman, A. *J. Biol. Chem.* **1994**, *264*, 6296−6305.
(9) Rees, B.; Bilwes, A. *Chem. Res. Toxicol.* **1993**, *6*, 385−406.
(10) Guenneugues, M.; Drevet, P.; Pinkasfeld, S.; Gilquin, B.; Ménez, A.; Zinn-Justin, S. *Biochemistry*, **1997**, *36*, 16097−16108.
(11) Szegletes, T.; Mallender, W. D.; Rosenberry, T. L. *Biochemistry* **1998**, *37*, 4206−4216.
(12) Weise, C.; Kreienkamp, H.-J.; Raba, R.; Pedak, A.; Aaviksaar, A.; Hucho, F. *EMBO J.* **1990**, *9*, 3885−3888.
(13) Radić, Z.; Pickering, N. A.; Vellom, D. C.; Camp, S.; Taylor, P. *Biochemistry* **1993**, *32*, 12074−12084.
(14) Radić, Z.; Duran, R.; Vellom, D. C.; Li, Y.; Cerveñansky, C.; Taylor, P. *J. Biol. Chem.* **1994**, *269*, 11233−11239.
(15) Bourne, Y.; Taylor, P.; Marchot, P. *Cell* **1995**, *83*, 503−512.
(16) Harel, M.; Kleywegt, G. J.; Ravelli, R. B.; Silman, I.; Sussman, J. L. *Structure* **1995**, *3*, 1355.
(17) Kryger, G.; Harel, M.; Giles, K.; Toker, L.; Velan, B.; Lazar, A.; Kronman, C.; Barak, D.; Ariel, N.; Shafferman, A.; Silman, I.; Sussman, J. L. *Acta Crystallogr., Sect. D* **2000**, *56*, 1385−1394.
(18) Radić, Z.; Quinn, D. M.; Vellom, D. C.; Camp, S.; Taylor, P. *J. Biol. Chem.* **1995**, *270*, 20391−20399.
(19) Eastman, J.; Wilson, E. J.; Cerveñansky, C.; Rosenberry, T. L. *J. Biol. Chem.* **1995**, *270*, 19694−19701.
(20) Rosenberry, T. L.; Rabl, C.-R.; Neumann, E. *Biochemistry* **1996**, *35*, 685−690.
(21) Szegletes, T.; Mallender, W. D.; Thomas, P. J.; Rosenberry, T. L. *Biochemistry* **1999**, *38*, 122−133.
(22) Tai, K.; Shen, T.; Henchman, R. H.; Bourne, Y.; Marchot, P.; McCammon, J. A. *J. Am. Chem. Soc.* **2002**, *124*, 6153−6161.
(23) Bui, J. M.; Tai, K.; McCammon, J. A. *J. Am. Chem. Soc.* **2004**, *126*, 7198−7205.
(24) Shi, J.; Tai, K.; McCammon, J. A.; Taylor, P.; Johnson, D. A. *J. Biol. Chem.* **2003**, *276*, 30905−30911.
(25) Radić, Z.; Taylor, P. *J. Biol. Chem.* **2001**, *276*, 4622−4633.
(26) Marchot, P.; Prowse, C. N.; Kanter, J.; Camp, S.; Achermann, E. J.; Radić, Z.; Bougis, P. E.; Taylor, P. *J. Biol. Chem.* **1997**, *272*, 3502−3510.
(27) Sobolev, V.; Sorokine, A.; Prilusky, J.; Abola, E. E.; Edelman, M. *Bioinformatics* **1999**, *15*, 327−332.
(28) Stites, W. E. *Chem. Rev.* **1997**, *97*, 1233−1250.
(29) Müller-Dethlefs, K.; Hobza, P. *Chem. Rev.* **2000**, *100*, 143−167.
(30) Jeffrey, G. A.; Saenger, W. *Hydrogen Bonding in Biological Structures*; Springer-Verlag Press: Berlin, New York, 1994.
(31) Liu, D.; Wyttenbach, T.; Carpenter C. J.; Bowers, M. T. *J. Am. Chem. Soc.* **2004**, *126*, 3261−3270.
(32) Stryer, L. *Biochemistry*; Freeman Press: New York, 1988.
(33) Williams, D. H.; Maguire, A. J.; Tsuzaki, W.; Westwell, M. S. *Science* **1998**, *280*, 711−714.
(34) Shiozawa, H.; Chia, B. C. S.; Davies, N. L.; Zerella, R.; Williams, D. H. *J. Am. Chem. Soc.* **2002**, *124*, 3914−3919.
(35) Williams, D. H.; Davies, N. L.; Zerella, R.; Bardsley, B. *J. Am. Chem. Soc.* **2004**, *126*, 2042−2049.
(36) Benkoussa, M.; Nomine, B.; Mouchon, A.; Lefebvre, B.; Bernardon, J. M.; Formstecher, P.; Lefebvre, P. *Recept. Signal Transduction* **1997**, *7*, 257−267.
(37) Freire, E. *Proc. Natl. Acad. Sci. U.S.A.* **1999**, *96*, 10118−10122.
(38) Roux, S.; Terouanne, B.; Couette, B.; Rafestin-Oblin, M. E.; Nicolas, J. C. *J. Biol. Chem.* **1999**, *274*, 10059−10065.
(39) Shoelson, S. E.; Sivaraja, M.; Williams, K. P.; Hu, P.; Schlessinger, J.; Weiss, M. A. *EMBO J.* **1993**, *12*, 795−802.
(40) Becke, A. D. *J. Chem. Phys.* **1993**, *98*, 5648−5652.
(41) Lee, C.; Yang W.; Parr, R. G. *Phys. Rev. B* **1988**, *37*, 785−789.
(42) Miehlich, B.; Savin, A.; Stoll, H.; Preuss, H. *Chem. Phys. Lett.* **1989**, *157*, 200−206.
(43) Hehre, W. J.; Radom, L.; Schleyer, P. R.; Pople, J. A. *Ab Initio Molecular Orbital Theory*; Wiley: New York, 1986.
(44) Mebel, A. M.; Morokuma, K.; Lin, C. M. *J. Chem. Phys.* **1995**, *103*, 7414−7421.
(45) Johnson, B. G.; Gill, P. M. W.; Pople, J. A. *J. Chem. Phys.* **1993**, *98*, 5612−5626.
(46) Wang, J.; Roszak, S.; Gu, J.; Leszczynski, J. *J. Phys. Chem. B* **2005**, *109*, 1006−1014.
(47) Gu, J.; Wang, J.; Leszczynski, J. *J. Am. Chem. Soc.* **2004**, *126*, 12651−12660.
(48) Spiner, J.; Leszczynski, J.; Hobza, P. *J. Phys. Chem.* **1996**, *100*, 1965−1974.
(49) Head-Gorden, M.; Pople, J. A.; Frisch, M. J. *Chem. Phys. Lett.* **1988**, *153*, 503.
(50) Frisch, M. J.; Head-Gordon, M.; Pople, J. A. *Chem. Phys. Lett.* **1990**, *166*, 275.
(51) Frisch, M. J.; Head-Gordon, M.; Pople, J. A. *Chem. Phys. Lett.* **1990**, *166*, 281.
(52) Frisch, M. J.; Trucks, G. W.; Schlegel, H. B.; Scuseria, G. E.; Robb, M. A.; Cheeseman, J. R.; Zakrzewski, V. G.; Montgomery, J. A., Jr.; Stratmann, R. E.; Burant, J. C.; Dapprich, S.; Millam, J. M.; Daniels, A. D.; Kudin, K. N.; Strain, M. C.; Farkas, O.; Tomasi, J.; Barone, V.; Cossi, M.; Cammi, R.; Mennucci, B.; Pomelli, C.; Adamo, C.; Clifford, S.; Ochterski, J.; Petersson, G. A.; Ayala, P. Y.; Cui, Q.; Morokuma, K.; Malick, D. K.; Rabuck, A. D.; Raghavachari, K.; Foresman, J. B.; Cioslowski, J.; Ortiz, J. V.; Stefanov, B. B.; Liu, G.; Liashenko, A.; Piskorz, P.; Komaromi, I.; Gomperts, R.; Martin, R. L.; Fox, D. J.; Keith, T.; Al-Laham, M. A.; Peng, C. Y.; Nanayakkara, A.; Gonzalez, C.; Challacombe, M.; Gill, P. M. W.; Johnson, B. G.; Chen, W.; Wong, M. W.; Andres, J. L.; Head-Gordon, M.; Replogle, E. S.; Pople, J. A. *Gaussian 98*, revision D.3; Gaussian, Inc.: Pittsburgh, PA, 1998.

(53) Bader, R. F. W. *Atoms in Molecules: A Quantum Theory* Clarendon Press: Oxford, U. K., 1990.
(54) Bader, R. F. W. *Chem. Rev.* **1991**, *91*, 893.
(55) Koch, U.; Popelier, P. L. A. *J. Phys. Chem.* **1995**, *99*, 9747.
(56) Popelier, P. L. A. *J. Phys. Chem. A* **1998**, *102*, 1873−1878.
(57) Biegler-König, F.; Schönbohm, J.; Bayles, D. *J. Comput. Chem.* **2001**, *22*, 545−559 (AIM2000 homepage: http://www.aim2000.de).
(58) Kitaura, K.; Morokuma, K. *Int. J. Quantum Chem.* **1976**, *10*, 325.
(59) Morokuma, K.; Kitaura, K. *Chemical Applications of Atomic and Molecular Electrostatic Potentials*; Politer, P., Truhlar, D. G., Eds.; Plenum Press: New York, 1981.
(60) Schmidt, M. W.; Baldridge, K. K.; Boatz, J. A.; Elbert, S. T.; Gordon, M. S.; Jensen, J. H.; Koseki, S.; Matsunaga, N.; Nguyen, K. A. *J. Comput. Chem.* **1993**, *14*, 1347.
(61) Cossi, M.; Barone, V.; Cammi, R.; Tomasi, J. *Chem. Phys. Lett.* **1996**, *255*, 327−335.